Published in final edited form as:
Nat Struct Mol Biol. 2008 October 01; 15(10): 1084–1093. doi:10.1038/nsmb.1492.

Mapping a Molecular Link between Allosteric Inhibition and Activation of the Glycine Receptor

Paul S. Miller[1], **Maya Topf**[2], **Trevor G. Smart**[1]

[1]Department of Pharmacology, University College London, Gower Street, London, WC1E 6BT, UK

[2]School of Crystallography, Birkbeck College, Malet Street, London, WC1E 7HX, UK

Abstract

Cys-loop ligand-gated ion channels mediate rapid neurotransmission throughout the central nervous system. They possess agonist recognition sites and allosteric sites where modulators regulate ion channel function. Using strychnine-sensitive glycine receptors, we identified a scaffold of hydrophobic residues enabling allosteric communication between glycine-agonist binding loops A and D, and the Zn^{2+} inhibition site. Mutating these hydrophobic residues disrupted Zn^{2+} inhibition, generating novel Zn^{2+} activated receptors and spontaneous channel activity. Homology modelling and electrophysiology revealed that these phenomena are caused by disruption to three residues on the '–' loop face of the Zn^{2+} inhibition site, and to D84 and D86, on a neighbouring β3 strand, forming a Zn^{2+} activation site. We provide a new view for the activation of a Cys-loop receptor where, following agonist binding, the hydrophobic core and interfacial loops reorganise in a concerted fashion to induce downstream gating.

The Cys-loop ligand-gated ion channel superfamily includes nicotinic acetylcholine (nAChR), γ-aminobutyric acid type A ($GABA_A$), glycine (GlyR) and serotonin type 3 ($5HT_3$) receptors. Each subunit of these pentamers contains: a ligand-binding extracellular domain (ECD), formed by a sandwich of two β-sheets; a four α-helical membrane-spanning domain; and an intracellular region of unspecified quaternary structure [1]. The interior of the ECD is hydrophobic[2,3], and, as for most globular proteins, it is considered to be an entropic stabiliser of protein folding [4]. Given the presumed stability of this hydrophobic core and its location between two sheets of rigid β-strands, it is usually regarded as a relatively inflexible structure. Thus, after agonist-induced activation, the core would move, if at all, as a rigid body [5]. Accordingly, it would be the agonist-binding loops A-F, supported by the surrounding rigid β-strands, that would undergo a conformational change upon agonist binding to trigger rigid body movement and downstream channel opening[2, 6, 7, 7–11]. An alternative view, based on structural and modelling data, suggests that substantial portions of the inner and outer β-sheets of the ECD shift their orientation relative to one another upon receptor activation[1, 12]. Given the location of the hydrophobic core between the inner and outer β-sheets of each ECD it would then be expected that the core would reorganise, rather

Proofs and correspondence to: Professor T.G. Smart, Department of Pharmacology, University College London, Gower Street, London, WC1E 6BT, Tel no 0044-207-679-3770, Fax no 0044-207-679-7298, t.smart@ucl.ac.uk.

Europe PMC Funders Author Manuscripts

than move as a rigid body, to facilitate the reorientation of the β-sheets [13–17]. This movement may induce separation of important charge interactions along neighbouring receptor subunit interfaces, allowing the ECDs to twist and induce downstream channel opening[8, 16, 18, 19].

An ideal model system to investigate the role of the hydrophobic core in Cys-loop receptor activation is that involving Zn^{2+} inhibition of the GlyR. These receptors readily form homomers that are modulated by the physiological cation Zn^{2+} in a biphasic fashion. Zn^{2+} can be found in nanomolar concentrations in external medium and is also packaged into vesicles and released at synapses in sufficient amounts to endogenously modulate GlyRs, with low micromolar concentrations potentiating submaximal glycine responses, and higher concentrations causing inhibition [20–22]. Two Zn^{2+} binding sites have been identified; the potentiation site is contained solely on the outer β sheet of the ECD [23], whereas the inhibition site spans neighbouring subunits on the inner β sheet of the ECDs [24,25,26] (Fig. 1a-c). Inhibition by Zn^{2+} of GlyR function involves the stabilisation of charge interactions between neighbouring subunit ECD interfaces, thereby hindering their movement. This supports the notion that charge separation of neighbouring ECD interfaces is necessary for receptor activation, and that agonist binding must transduce a signal near to the Zn^{2+} inhibition site to evoke a conformational change in this area leading to receptor activation. As the hydrophobic core is located between the glycine binding site and the Zn^{2+} inhibition site, identifying the molecular requirements for Zn^{2+} inhibition will elucidate the roles of the hydrophobic core and the subunit ECD interface in receptor function.

Here, we demonstrate that a cluster of residues forming a scaffold across the hydrophobic core are critical for Zn^{2+} inhibition and spontaneous opening of the *human* GlyR ion channel. Spontaneous opening was attributed to the apparent flexibility of a loop on the '–' face of the Zn^{2+} inhibition site, which is exquisitely-sensitive to the molecular composition of the hydrophobic core. Disruption of this loop and the discovery of novel elements in a neighbouring β3 strand that are also important for receptor activation, demonstrate that charge redistribution at the ECD inner subunit interface is a key component of GlyR activation.

Results

Hydrophobic residues are required for Zn^{2+} inhibition

A GlyR homology model was constructed to guide our site-directed mutagenesis studies into receptor activation. The GlyR protein sequence was first aligned with other Cys-loop receptors, revealing that the region encompassing the GlyR Zn^{2+} inhibition site is not conserved across any of the Cys-loop receptors, for which atomic resolution ECD templates are available, and furthermore, it contains a 2 – 3 amino acid insertion. Structural alignment of three ECD template structures (conotoxin-bound *Aplysia californica* acetylcholine binding protein, (Ctx-Ac-AChBP [27]); *Torpedo* (*Tor*) nAChR α_1 [1]; and *mouse* nAChR α1 subunit [14]), revealed substantial structural variation at the two loops of the '+' and '–' face [28] flanking the β5 strand (nomenclature of Brejc [2]; Supplementary Fig. 1), which corresponds to the Zn^{2+} inhibition site. Using the variable loop regions as insertion points for the extra residues in our GlyR alignment (Fig. 1a) allowed us to generate a GlyR homology model

(MODELLER-9.2 [29]; based on the *Tor*nAChR α_1 template) with His107 and His109 exposed at the subunit interface [25] and Phe108 solvent accessible [30], in accord with published data.

To probe the link between Zn^{2+} inhibition and GlyR activation, hydrophobic residues positioned between the Zn^{2+} inhibition site, defined by His107, His109, Thr112 and Thr133 [24, 26, 31], and the three closest agonist binding loops (A, D and E; Fig. 1b,c), were substituted with alanine. Substituted GlyRs were expressed in human embryonic kidney (HEK) cells and their sensitivities to Zn^{2+} potentiation and inhibition assessed by whole-cell recording of glycine (EC_{50}) evoked responses in the presence of increasing concentrations of Zn^{2+}. Substituting residues at the Zn^{2+} inhibition site '–' face (β5 F108A, I111A; β6' I132A, L134A) and the loop A face (L98A, F99A, F100A), substantially reduced sensitivity to Zn^{2+} inhibition compared to wild-type, whilst Zn^{2+} potentiation remained the same (Fig. 1d,e). Substitutions in agonist binding loop D (V60A, I62A, L64A) also reduced Zn^{2+} inhibition with I62A causing ablation. This residue is orientated in the GlyR model towards other residues required for Zn^{2+} inhibition from loop A (Leu98, Phe99, Phe100) and those from β5 and β6' adjoining the Zn^{2+} inhibition site (Phe108, Ile111, Ile132, Leu134). By contrast, substituting distally-located hydrophobic residues in agonist-binding loop E (Leu117 and Leu118; Fig. 1e and Table 1), and other hydrophobic residues located away from loops A/D and β5/6' (Supplementary Fig. 3 and Supplementary Table 1), did not disrupt Zn^{2+} inhibition. All the substituted receptors with attenuated Zn^{2+} inhibition retained glycine EC_{50}s within 10-fold of the wild-type (Table 1) and comparable maximal glycine currents (I_{max}) and Hill slopes, with the exception of $\alpha1^{F99A}$ (I_{max} = 3.9 ± 0.4 nA; wild-type GlyR I_{max} = 6.8 ± 0.5 nA; P < 0.01).

Removing Zn^{2+} inhibition creates Zn^{2+}-activated GlyRs

Although Zn^{2+} does not activate wild-type $GABA_A$ or glycine receptors, it generated inward currents at GlyRs with impaired Zn^{2+} inhibition, i.e., those with alanine substitutions in the glycine binding loops A/D and Zn^{2+} inhibition binding strands β5/6' (L98A, F99A, F100A, F108A, I111A, I132A, L134A, I62A and I64A; Fig. 2a). The Zn^{2+}-activated currents reversed close to E_{Cl} (0.4 ± 1.4 mV, n = 5), and the current-voltage relationships were comparable to those for glycine-activated Cl^- currents at wild-type GlyRs (Fig. 2b). Zn^{2+} concentration response curves revealed that the potency and relative efficacy (maximal Zn^{2+} response as a percentage of maximal glycine response in the same cell), varied substantially between the substituted receptors (Fig. 2c and Table 1). $\alpha1^{L134A}$ exhibited the highest sensitivity to Zn^{2+} (EC_{50} = 0.06 ± 0.01 μM, n = 5), whilst $\alpha1^{F99A}$ exhibited the highest relative efficacy (86 ± 13%, n = 5). By contrast, $\alpha1^{I62A}$ supported only 3 ± 1% maximal activation with 1 mM Zn^{2+} (Fig. 2c and Table 1). Entirely consistent with Zn^{2+} activating the substituted GlyRs, the anion-selective channel blocker, cyanotriphenylborate (CTB, 20 μM), abolished the Zn^{2+}-activated currents (Fig. 2d). Furthermore, both strychnine, a selective GlyR competitive antagonist, and picrotoxin (PTX), a $GABA_A$R and GlyR allosteric blocker, also inhibited Zn^{2+} activation (Fig. 2e,f). This prompted the classification of these substituted GlyRs as Zn^{2+}-activated GlyRs (ZAGs).

Hydrophobicity and sensitivity to Zn^{2+} inhibition

To investigate the ZAGs further, we substituted loop A, Phe99 and Phe100, and β5 Phe108 (Fig. 3a) individually with either: tyrosine or tryptophan – both aromatic like Phe; or leucine or methionine – aliphatic. Although many substitutions reduced Zn^{2+} inhibition (Fig. 3b-d), only some generated ZAG behaviour (Fig. 3e-g). Of the three Phe residues, Phe100 is the most critical for maintaining wild-type sensitivity to Zn^{2+} inhibition; however, there was no correlation between the properties of the substituting residue and the disruption to Zn^{2+} inhibition (Fig. 3b-d and Supplementary Table 2), suggesting each position has unique chemical and physical requirements.

Glycine EC_{50}s for α1 Phe100 and Phe108 substituted receptors remained within two-fold of wild-type with the exceptions of $\alpha1^{F100Y}$ and $\alpha1^{F108W}$ (increased 15- and 25-fold, respectively; *P<0.05*; Supplementary Table 2). For Phe99 substituted receptors, glycine EC_{50}s were significantly increased for $\alpha1^{F99L}$, $\alpha1^{F99W}$ and $\alpha1^{F99Y}$ (3- to 30-fold; *P<0.05*), but surprisingly the $\alpha1^{F99M}$ receptor was 6-fold more sensitive to glycine (wild-type EC_{50} = 35 ± 5 μM; $\alpha1^{F99M}$ EC_{50} = 5.5 ± 0.5 μM, n = 4 – 6; *P<0.05*), suggesting an important role for this residue in determining glycine binding. Interestingly, the GlyR model positions Phe99 facing into the glycine binding site (Fig. 1b,c).

Zn^{2+} activation originates from a novel binding site

The switch from Zn^{2+} inhibition to activation in ZAGs could have arisen if the function of an existing modulatory Zn^{2+} binding site was altered enabling activation in response to Zn^{2+} binding. However, substitution of Zn^{2+} binding residues with non-Zn^{2+} coordinating alanines at either the Zn^{2+} inhibition or potentiation sites revealed that neither site was required for Zn^{2+} activation (Supplementary Fig. 4). However, given that Zn^{2+} inhibition was severely compromised in ZAGs, we reasoned that regions bordering the inhibition site may have become structurally perturbed, sufficient to form a new Zn^{2+} activation site.

On an $\alpha1^{L134A}$ ZAG background (most Zn^{2+}-sensitive ZAG), potential Zn^{2+} coordinating residues neighbouring the Zn^{2+} inhibition site were substituted with alanine and assessed for activation by 0.1 μM Zn^{2+} (EC_{70} for $\alpha1^{L134A}$; Fig. 4a,b). Of these substitutions, Asp84, Asp86 (strand β3) and Asp97 (loop A) virtually abolished Zn^{2+} activation from 38 ± 9% ($\alpha1^{L134A}$) to 5 ± 1% ($\alpha1^{L134A, D84A}$) and 2.4 ± 1.2% ($\alpha1^{L134A, D86A}$), with no detectable activation for $\alpha1L^{L134A, D97A}$ (Fig. 4c). The Zn^{2+} EC_{50}s for $\alpha1^{L134A, D84A}$ and $\alpha1^{L134A, D86A}$ were increased 120- and 15-fold, respectively (Fig. 4c inset); whilst glycine EC_{50}s were only shifted 2-fold (Supplementary Table 3). Notably, using a wild-type receptor background, the substitutions D84A, D86A or D97A, caused only modest (< 2-fold) changes in GlyR sensitivity to Zn^{2+} inhibition and potentiation (Supplementary Fig. 5 and Supplementary Table 4).

According to the GlyR homology model (Fig. 4a), Asp84 and Asp86 are positioned approximately 17 Å from Asp97, which is too far for the three residues to coordinate a single Zn^{2+} ion [32]. Furthermore, Asp97, which is conserved across the Cys-loop receptor family, probably supports loop B via the carboxyl side chain [33], precluding its involvement in Zn^{2+} binding. To establish the importance of Asp84, Asp86 and Asp97 for Zn^{2+}

activation, alanine substitutions were also made on an alternative ZAG background, $\alpha1^{F99A}$ (most efficacious ZAG). Substituting Asp84 or Asp86 again substantially reduced the sensitivity to Zn^{2+} activation, but substituting Asp97 was ineffective (Fig. 4d). Thus, the role of Asp97 in Zn^{2+} activation is more complex than just directly binding Zn^{2+}.

Zn^{2+} activation site is not a potentiation site

As reagents and water are ubiquitously contaminated with glycine (~ 50 nM [34]), it is feasible that Asp84/Asp86 may actually form part of a (second) Zn^{2+} potentiation site, rather than an activation site. Occupancy of this site by Zn^{2+} would then enhance the receptor's sensitivity to glycine allowing activation by very low contaminating glycine concentrations. To address this, an $\alpha1^{L134A}$ ZAG background was used with an extra mutation, E157A on glycine binding loop B[35], to produce a receptor with 50-fold reduced sensitivity to glycine. The threshold concentration for glycine was now >100 μM (Fig. 5a) and 2000-fold higher than the predicted level of glycine contamination. Nevertheless, the $\alpha1^{L134,E157A}$ ZAG showed only a modest 3-fold reduced sensitivity to Zn^{2+} activation (Fig. 5b) and retained comparable maximal responses to Zn^{2+} (Fig. 5c). Using an alternative F99A background, $\alpha1^{F99A,E157A}$ yielded identical Zn^{2+} sensitivity to $\alpha1^{F99A}$, despite being insensitive up to 10 mM glycine (Fig. 5d,e). Thus, in the absence of glycine-mediated activation, Zn^{2+} activation is still apparent, suggesting it originates from a pure activation site, not an additional Zn^{2+} potentiation site.

ZAGs exhibit spontaneous channel activity

HEK cells expressing the most sensitive ZAGs, $\alpha1^{L98A}$, $\alpha1^{F99A}$, $\alpha1^{F108A}$ and $\alpha1^{L134A}$, all exhibited sizable (0.5 – 3 nA) leak currents. A minor component was caused by Zn^{2+} contamination of the external solution (~200 nM [36]) activating the ZAGs, as this was reduced by the Zn^{2+} chelators, tricine (2.5 mM) or *N,N,N′,N′*-tetrakis-(2-pyridylmethyl)-ethylenediamine (TPEN; 100 μM; Fig. 6a, b). The remaining component depended on spontaneous GlyR channel activity since it was abolished by CTB (20 μM) to less than 50 pA standing current (considered full abolition of receptor-mediated leak). Strychnine also attenuated the leak, by 100 % for ZAG $\alpha1^{F99A}$ and by 90 ± 4% for $\alpha1^{L134A}$. Strychnine was 10-fold less potent inhibiting the leak current compared to glycine-activated currents (Fig. 6c, d).

Interestingly, Asp84 and Asp86, which are important for Zn^{2+} activation, were also required for spontaneous activation with $\alpha1^{F99A,\ D84A}$, $\alpha1^{F99A,\ D86A}$, $\alpha1^{L134A,\ D84A}$, and $\alpha1^{L134A,\ D86A}$ failing to exhibit spontaneous channel activity (Fig. 6e). Furthermore, Asp84 and Asp86 also influenced glycine-induced receptor activation, as alanine substitutions induced a modest but consistent 2-fold reduction in glycine sensitivity of wild-type, $\alpha1^{F99A}$ and $\alpha1^{L134A}$ backgrounds (Fig. 6d and Supplementary Table 4). A double substituted receptor, $\alpha1^{D84A,\ D86A}$, was non-functional.

To investigate whether spontaneous activity mimics agonist-induced activity, single channel currents were recorded in cell-attached mode (pipette potential +60 mV) for wild-type channels activated by glycine (20 μM; EC_{30}) and for spontaneously-gating $\alpha1^{F99A}$ ZAGs without glycine. TPEN (100μM) was present throughout to remove any activation by

contaminating Zn^{2+}. The single channel currents for each receptor population were comparable at 4 – 5 pA with estimated conductances of ~ 60 pS [37] (Fig. 7a). The corresponding open time distributions were best fit by three Gaussian components with similar mean time constants and relative areas ($P > 0.05$; Fig. 7b and Table 2). The shut time distributions required five Gaussian components giving similar time constants for both receptors, with the exception of τ_{C2} and τ_{C3}, which were 2-fold higher for $\alpha1^{F99A}$ receptors (Fig. 7c and Table 2). These changes will contribute to the lower open probability (P_O) for clusters of openings at $\alpha1^{F99A}$ (0.53 ± 0.07) compared to wild type (0.9 ± 0.03, n = 3) channels. With regard to the burst duration distributions, four Gaussian components were required with comparable time constants and relative areas, except for τ_{B3}, which was 2-fold longer for $\alpha1^{F99A}$ (Fig. 7d).

The '–' face affects Zn^{2+} activation and spontaneous activity

Conceivably, Zn^{2+} activation and spontaneous channel activity may arise if the substitutions of hydrophobic residues exert a common conformational effect on a region that undergoes critical movement during channel gating. As the Zn^{2+} inhibition site is perturbed in ZAGs, it is the ideal region to examine for conformational flexibility. The top ten GlyR homology models (lowest distant-dependent atomic statistical potential (DOPE)[38] score from 100 models run in MODELLER-9.2) based on three related template structures, conotoxin-bound Ac-AChBP, *Tor*nAChR α_1 and mnAChR α1 [1, 14, 27], showed much greater structural variability at the '+' and '–' loop faces surrounding the β5 strand of the Zn^{2+} inhibition site, compared to other more rigid β-strands and across the structure as a whole (Fig. 8a, **insets** and Supplementary Table 5). By using DOPE loop modelling to optimise the structures of the GlyR '+' and '–' face loops, using *Tor*nAChR α_1 and mnAChR α1 as templates, the ten best conformations for the '+' loops were all comparable (Fig. 8b), whereas for the '–' face loops, variable conformations were equally favoured with residues exhibiting multiple orientations at this location (Fig. 8b and Supplementary Table 6).

To corroborate the modelling data, polar residues Thr112, Thr113 and Asp114 on the apex of the '–' face, the point of greatest variability between DOPE loop-fitted structures, were individually substituted with alanine and examined for Zn^{2+} activation and spontaneous activity. Although T112A yielded a highly-sensitive and efficacious ZAG (Fig. 8c), no single alanine substitution generated a spontaneously-active receptor (data not shown). We altered the apex flexibility of the '–' face by individually substituting Thr112, Thr113 and Asp114 with either glycine to increase, or proline to reduce, backbone flexibility [39, 40]. Whilst the proline-substituted receptors lacked spontaneous activity, two glycine-substituted receptors, $\alpha1^{T113G}$ and $\alpha1^{D114G}$, exhibited 15 ± 4% and 43 ± 10% (n = 4 – 6) spontaneous activity, respectively (Fig. 8d). Furthermore, there was a 3–fold increase in glycine sensitivity for $\alpha1^{T113G}$ (EC_{50} = 9 ± 2 μM) and $\alpha1^{D114G}$ (EC_{50} = 10 ± 3 μM) compared to WT (EC_{50} = 35 ± 5 μM; n = 4–6); whereas the proline substituted receptors all exhibited reduced sensitivities to glycine (Fig. 8e). Thus, increasing the flexibility of the '–' face around Thr112–Asp114 increased the propensity of GlyR to open spontaneously, and in response to agonist binding, while decreasing flexibility by proline substitution had the opposite effect.

Discussion

This study identifies a scaffold of hydrophobic residues in the GlyR that functionally link glycine binding loops A and D with the Zn^{2+} binding β5 and β6' strands of the Zn^{2+} inhibition site. Exchanging the hydrophobic residues, but not others outside the scaffold, initiated spontaneous channel opening, severely attenuated Zn^{2+} inhibition, and enabled Zn^{2+} to act as a novel activator of GlyRs. This suggests the hydrophobic scaffold is pivotally involved in receptor activation by stabilising one or more closed GlyR conformations. This is achieved by regulating the '–' loop face of the Zn^{2+} inhibition site, as specific substitutions of polar residues in the '–' face produced receptors with the same properties to those generated by alanine substitutions in the hydrophobic scaffold.

Structurally linking two discrete ligand binding sites

The current view of Cys–loop receptor activation is that agonist binding at the interface between subunits induces a rearrangement of interacting residues allowing the ECDs to twist relative to one another. The newly–orientated loops at the bases of the ECDs then promote rearrangement of opposing transmembrane domains to open the channel [6, 16, 18, 41–44]. By binding to its interfacial inhibitory site on GlyRs, Zn^{2+} stabilises subunit interfaces, preventing the ECDs from twisting and initiating activation. It is therefore plausible that by distorting the Zn^{2+} binding '–' loop interface we will not only ablate Zn^{2+} inhibition, but also enable spontaneous channel activity, particularly if the distortion mimics the conformation that occurs in the activated receptor state. Thus, the attenuation of Zn^{2+} inhibition and appearance of spontaneous channel activation are intrinsically linked. The extent to which both properties are seen in mutated receptors, will depend on the degree by which each substitution perturbs the '–' loop away from a closed towards an activated conformation.

Notably, the molecular pathway by which Zn^{2+} causes inhibition is entirely different to that for Zn^{2+} potentiation at GlyRs. The potentiation site resides very close to the Cys–loop where it may interact directly with Thr151 to facilitate channel gating [23]. This negates the need for any interaction with the hydrophobic scaffold identified here, explaining why Zn^{2+} potentiation was unaffected in this study.

The molecular pathway identified here is the first to be described in a Cys–loop ligand–gated ion channel that functionally connects two distinct binding sites, linking the agonist binding site to downstream activation. The importance of the hydrophobic scaffold in mediating GlyR activation is emphasised by the common kinetics of spontaneously–active $\alpha1^{F99A}$ and agonist–activated wild–type GlyRs. Specifically, for $\alpha1^{F99A}$, it is the alanine substitution that artificially perturbs loop A to induce activation, whilst for wild–type GlyRs it is presumably agonist binding that similarly perturbs loop A to cause activation. Although a critical role for loop A in directing receptor activation is evident for $GABA_A$Rs [45] and nAChRs [46], loop C, possibly *via* transmission of a conformational change along the outside of the ECDs (β7, 9 and 10 strands), has also been suggested to mediate activation upon agonist binding [8, 10]. Our data does not preclude this scenario, but advocates loop A as an important contributor to the conformational wave that precedes channel opening [47].

At the glycine binding site, Phe99 appears ideally positioned to directly influence the receptor's sensitivity to glycine, possibly via a cation–π interaction [48]. The action of Phe99 to induce GlyR activation in response to agonist binding may then be mediated *via* the hydrophobic scaffold and subsequent '–' loop face of the Zn^{2+} inhibition site. Indeed, Phe99 probably does this *via* Leu98 and Phe100, which are predicted to face, opposite to Phe99, into the hydrophobic scaffold towards the residues supporting the '–' face loop. Such an interaction with Phe99 would explain why Phe100 could also influence the receptor's sensitivity to glycine (Supplementary Figure 6; Supplementary Table 2). The ability of Phe99 to influence important residues within the hydrophobic scaffold may explain why it produces the most efficacious ZAG and the most spontaneously–active receptors when substituted with alanine.

From the perspective of the polar residues at the Zn^{2+} site's '–' loop face, substituting Thr112 or Ile111 produced a receptor that was insensitive to Zn^{2+} inhibition (cf [25, 31]) and capable of Zn^{2+} activation. Isoleucine 111 faces into the core, in close proximity with the other residues comprising the hydrophobic scaffold. Thus Thr112, *via* Ile111, is ideally located to act as a relay following perturbation of the hydrophobic scaffold. Sequential substitution of Thr113 and Asp114 within the '–' loop by glycine, but not by alanine or proline, also yielded spontaneously–active receptors. These residues must also be ideally located to respond to perturbations of the hydrophobic scaffold, with increased loop flexibility enabling the receptor to shift to an activated state, while imposed rigidity (e.g., proline insertion or when Zn^{2+} binds to stabilise this region) hinders receptor activation.

β5 loop movement during GlyR activation

Although we propose that the '–' face loop undergoes a conformational change to facilitate receptor activation, comparative structural evidence does not, so far, support this idea. Overlaying crystal structures of *Aplysia californica* AChBP bound to either α–conotoxin PnIA ('inactive conformation') or HEPES ('active conformation' [27]) does not reveal any variation around the corresponding '–' face loop region in the GlyR model (Supplementary Figure 7). Furthermore, structurally aligning *Torpedo* nAChR α_1 and α_2 subunits (presumed closed conformation), compared to β, δ and γ subunits (presumed open) for the pentamer, reveals only a small degree of variability around the corresponding '–' face loop region (Supplementary Figure 8). Of course, as static structures, it is possible that neither the HEPES–bound AChBP nor βδγ *Tor*AChR subunits represent fully–activated receptors. Alternatively, they might undergo different conformational rearrangements after activation compared to GlyRs. Simulation studies on nAChRs also do not support movements in the '–' face region [49], although the nanosecond timescales for these studies are as yet too short to encompass all conformational rearrangements in pentameric Cys–loop receptors.

Despite the caveats, the '–' loop face of the GlyR Zn^{2+} inhibition site was predicted to adopt multiple conformations and side chain orientations with the potential to influence receptor function. Moreover, previous functional studies support a role for the '–' face loop in the GlyR activation process, notably: Thr112 is important in determining partial agonist efficacy [50]; it is accessible to Cys–scanning mutagenesis, resulting in dynamic disruption to agonist–evoked responses [30]; and Zn^{2+} binds between subunits at the '–' loop face to stabilise the

GlyR closed conformation, suggesting this interface is mobile during receptor activation [25, 31].

Creating a Zn^{2+} activation site

The Zn^{2+} activation site was localised to Asp84/Asp86 on strand β3, directly above the '–' face loop. Structural perturbation of the '–' loop face may therefore have a knock–on effect on the β3 region, allowing Asp84/Asp86 to form a novel Zn^{2+} binding site that aids movement of the subunit interfaces, rather than hinders them, so inducing activation. This provides further evidence that charge dispersal at subunit interfaces plays an important role in regulating Cys–loop receptor excitability [16, 19, 46, 51], and also indicates that a dynamic interaction occurs between the '–' loop face and the β3 strand to facilitate activation of wild–type receptors. The variable potency and efficacy of Zn^{2+} at different ZAGs further indicates that hydrophobic residues within the scaffold differentially affect the '–' loop face, and consequently the juxtaposed β3 strand, so determining the efficiency with which Asp84/Asp86 forms a new Zn^{2+} activation site.

The general activation mechanism presented here for the GlyR is in accord with the hydrophobic scaffold and '–' face loop dynamically responding to agonist binding. This provides a new vista on Cys–loop receptor activation whereby, during activation, the reorganisation of the hydrophobic scaffold and '–' face facilitate the re–alignment of the inner and outer β–sheets relative to one another [12, 13, 16, 18]. This then initiates movement of subunit interfaces, which is subsequently transmitted to the transmembrane domains for receptor activation [42].

Methods

cDNA constructs and mutagenesis

We used *human* (h) GlyR α1L cDNA constructs and the mutant cDNAs were prepared using the Stratagene Quikchange kit. Mutated cDNAs were sequenced using an ABI sequencer.

Cell culture, transfection and electrophysiology

By using a calcium phosphate transfection method (3 GlyR α1:1 eGFP) we expressed GlyR in HEK cells (ATCC CRL1573) grown on poly–L–Lysine–coated coverslips at 10% confluence. Whole–cell membrane currents were recorded after 24 h at 20–22°C from single HEK cells held at –40 mV using the patch clamp technique (Axopatch 200B, Molecular Devices). For rapid drug applications (exchange rate ~50–100 ms), we used a Y–tube. Patch electrodes (4 – 5 MΩ) were filled with (mM): 140 KCl, 2 $MgCl_2$, 1 $CaCl_2$, 10 HEPES, 11 EGTA, and 2 ATP, pH 7.2 (≈ 300 mOsm). External solution contained (mM): 140 NaCl, 4.7 KCl, 1.2 $MgCl_2$, 2.5 $CaCl_2$, 10 HEPES, and 11 D–Glucose, pH 7.4 (≈ 300 mOsm). For GlyRs exhibiting nanomolar sensitivities to Zn^{2+} activation, the tricine (2.5 mM; Zn^{2+} complexation $K_D = 10^{-5}$ M, ref. [52]), was added to the saline to remove Zn^{2+} contamination [36]. For single channel analysis, thick–walled electrodes were used (10 – 20 MΩ) and filled with external saline solution containing 100 μM TPEN, and 10 mM TEA to block endogenous potassium channel activity. Single–channel recordings were made in cell–attached mode at +60 mV pipette potential.

Data acquisition and analysis

Membrane currents were filtered using a high–pass Bessel filter at 3 kHz (–36dB per octave) and series resistance compensation was routinely achieved up to 70%. Data were recorded in 20 s epochs directly to a Pentium IV, 3.5 GHz computer into Clampex 8.0 via a Digidata 1322A (Axon instruments) sampling at 200 μs intervals. Due to Zn^{2+} activation in many of the receptors, Zn^{2+} inhibition profiles were measured by prolonged (4 s) co–application of Zn^{2+} with glycine, with response measurements being taken at the 4 s time point (to allow Zn^{2+} inhibition sufficient time to reach equilibrium [26]). The digitised membrane current records were analysed offline using Axoscope 8.2. The concentration response relationships for glycine and Zn^{2+} were fitted with modified Hill equations as previously described [26].

For the single channel data analyses, stored pre–filtered (2.7 kHz Bessel) single channel data were digitised at 33 kHz prior to analysis. A fixed time resolution based on the dead time of the system was set at 80 μs. The analysis of the single channel current amplitudes was performed by fitting Gaussian components to the amplitude distributions to determine the mean single channel current, standard deviation and the total area of the component using a non–linear least–squares fitting routine. Single–channel conductances were calculated from the mean unitary current and the difference between the patch potential and glycine response reversal potential. The patch potential was estimated in cell–attached recordings, by estimating the cell membrane potential.

All open and shut durations were measured with a 50% threshold cursor applied to the main single channel current amplitude (WinEDR v2.8.9). The duration of events that were included in the analysis was not less than 200 μs before fitting the dwell time histograms. Frequency distributions were constructed from the measured individual open and shut durations and analysed by fitting a mixture of exponentials, defined by:

$$y(t) = \sum_{i=1}^{n} (A_i/\tau_i) \cdot \exp(-t/\tau)$$

where A_i represents the area of the i^{th} component to the distribution and τ_i represents the respective time constant. The areas, time constants and standard errors of the individual components of the distribution were determined. The burst duration analysis required the determination of a critical shut time (τ_{crit}) [53] determined between the shut time constants, τ_{C3} and τ_{C4} by solving:

$$\exp(-t_{crit}/\tau_{C3}) = 1 - \exp(-t_{crit}/\tau_{C4})$$

Channel open probability (P_O) was calculated as the percentage of time that the channel spent in the open state within a cluster. All statistical comparisons used an unpaired t test and $P<0.05$ was considered significant.

Homology and loop modelling

We used ClustalW [54] to produce protein sequence alignments. A*plysia californica* acetylcholine binding protein, Ac–AChBP (2br8 [27]; conotoxin–bound form), *Torpedo* (*Tor*)nAChR $\alpha_1\beta\delta\alpha_2\gamma$ (2BG9) [1], and *mouse* (m)nAChR α1 (2QC1 [14]) were used for the Combinatorial Extension (CE) structural alignment method [55], which helped identify divergent regions in the GlyR α1 model. The final alignment reflected both alignment strategies. The *Torpedo* nAChR α_1 subunit was selected as the final template structure to guide the homology modelling of the GlyR α subunit, as it has only two less residues around the β5 strand (the GlyR Zn^{2+} inhibition site), compared to three less residues for Ac–AChBP; and also, the structure of *Tom*nAChR α_1 was determined as part of a pentamer, whereas mnAChR α1 was crystallized as a non–physiological monomer with several artificial point mutations [14]. The *Tom*nAChR α_1 pentamer was built by overlaying a second α_1 subunit over the α_2 subunit and then using Chimera [56], to build a five–fold symmetric pentamer. Using MODELLER–9.2 [29], 100 hGlyR α1 models were generated with Cys bridges added into the agonist binding loop C (C198–C209), for the principle *Tom*nAChR α_1 pentamer template, and also for the Ac–AChBP–conotoxin–bound pentamer and mnAChR α1 monomer. Side chain configurations were generated using SCWRL3 [57]. Fifty loops were generated using DOPE loop modelling in Modeller 9.2, for each loop before (‘+’) and after (‘–’) the β5 strand for each of the subunit templates (‘+’ loop residues ^{102}NEKGAH^{107}; ‘–’ loop residues ^{110}EITTDN^{115}). Models were evaluated using MolProbity [58] and gave good general agreement with each other. Uncertainty regarding the short β5 strand, ascribed as a β–strand in Ac–AChBP (1UW6) and nAChR α1 (2QC1), but not in *Tom*nAChR α_1 (2BG9), was considered unimportant, as it had little effect on side chain positioning, and a PSIPRED [59] secondary structure prediction of the GlyR sequence gave low confidence for the presence of a β–strand, suggesting neither one nor other template was more likely to be correct. All 3–D images were prepared and rendered using Chimera [56].

Supplementary Material

Refer to Web version on PubMed Central for supplementary material.

Acknowledgements

This work was supported by the MRC, BBSRC and the Wellcome Trust. We thank Alastair Hosie, Philip Thomas and Megan Wilkins for helpful comments and Helena Da Silva for technical assistance.

References

1. Unwin N. Refined structure of the nicotinic acetylcholine receptor at 4A resolution. J Mol Biol. 2005; 346:967–989. [PubMed: 15701510]
2. Brejc K, et al. Crystal structure of an ACh–binding protein reveals the ligand–binding domain of nicotinic receptors. Nature. 2001; 411:269–276. [PubMed: 11357122]
3. Chen Y, Reilly K, Chang Y. Evolutionarily conserved allosteric network in the Cys loop family of ligand–gated ion channels revealed by statistical covariance analyses. J Biol Chem. 2006; 281:18184–18192. [PubMed: 16595655]
4. Chandler D. Interfaces and the driving force of hydrophobic assembly. Nature. 2005; 437:640–647. [PubMed: 16193038]

5. Corringer PJ, Le NN, Changeux JP. Nicotinic receptors at the amino acid level. Annu Rev Pharmacol Toxicol. 2000; 40:431–458. [PubMed: 10836143]
6. Lester HA, Dibas MI, Dahan DS, Leite JF, Dougherty DA. Cys–loop receptors: new twists and turns. Trends Neurosci. 2004; 27:329–336. [PubMed: 15165737]
7. Sine SM, Engel AG. Recent advances in Cys–loop receptor structure and function. Nature. 2006; 440:448–455. [PubMed: 16554804]
8. Law RJ, Henchman RH, McCammon JA. A gating mechanism proposed from a simulation of a human alpha7 nicotinic acetylcholine receptor. Proc Natl Acad Sci U S A. 2005; 102:6813–6818. [PubMed: 15857954]
9. Celie PH, et al. Nicotine and carbamylcholine binding to nicotinic acetylcholine receptors as studied in AChBP crystal structures. Neuron. 2004; 41:907–914. [PubMed: 15046723]
10. Lyford LK, Sproul AD, Eddins D, McLaughlin JT, Rosenberg RL. Agonist–induced conformational changes in the extracellular domain of alpha 7 nicotinic acetylcholine receptors. Mol Pharmacol. 2003; 64:650–658. [PubMed: 12920201]
11. McLaughlin JT, Fu J, Sproul AD, Rosenberg RL. Role of the Outer beta–Sheet in Divalent Cation Modulation of {alpha}7 Nicotinic Receptors. Mol Pharmacol. 2006; 70:16–22. [PubMed: 16533908]
12. McLaughlin JT, Fu J, Rosenberg RL. Agonist–driven conformational changes in the inner beta–sheet of alpha7 nicotinic receptors. Mol Pharmacol. 2007; 71:1312–1318. [PubMed: 17325129]
13. Purohit P, Auerbach A. Acetylcholine receptor gating: movement in the alpha–subunit extracellular domain. J Gen Physiol. 2007; 130:569–579. [PubMed: 18040059]
14. Dellisanti CD, Yao Y, Stroud JC, Wang ZZ, Chen L. Crystal structure of the extracellular domain of nAChR alpha1 bound to alpha–bungarotoxin at 1.94 A resolution. Nat Neurosci. 2007; 10:953–962. [PubMed: 17643119]
15. Chakrapani S, Bailey TD, Auerbach A. Gating dynamics of the acetylcholine receptor extracellular domain. J Gen Physiol. 2004; 123:341–356. [PubMed: 15051806]
16. Unwin N, Miyazawa A, Li J, Fujiyoshi Y. Activation of the nicotinic acetylcholine receptor involves a switch in conformation of the alpha subunits. J Mol Biol. 2002; 319:1165–1176. [PubMed: 12079355]
17. McLaughlin JT, Fu J, Rosenberg RL. Agonist–driven conformational changes in the inner beta–sheet of alpha7 nicotinic receptors. Mol Pharmacol. 2007; 71:1312–1318. [PubMed: 17325129]
18. Taly A, et al. Implications of the quaternary twist allosteric model for the physiology and pathology of nicotinic acetylcholine receptors. Proc Natl Acad Sci U S A. 2006; 103:16965–16970. [PubMed: 17077146]
19. Mukhtasimova N, Sine SM. An intersubunit trigger of channel gating in the muscle nicotinic receptor. J Neurosci. 2007; 27:4110–4119. [PubMed: 17428989]
20. Hirzel K, et al. Hyperekplexia phenotype of glycine receptor alpha1 subunit mutant mice identifies Zn(2+) as an essential endogenous modulator of glycinergic neurotransmission. Neuron. 2006; 52:679–690. [PubMed: 17114051]
21. Bloomenthal AB, Goldwater E, Pritchett DB, Harrison NL. Biphasic modulation of the strychnine–sensitive glycine receptor by Zn^{2+} Mol Pharmacol. 1994; 46:1156–1159. [PubMed: 7808436]
22. Laube B, et al. Modulation by zinc ions of native rat and recombinant human inhibitory glycine receptors. J Physiol. 1995; 483(Pt 3):613–619. [PubMed: 7776247]
23. Miller PS, Da Silva HM, Smart TG. Molecular basis for zinc potentiation at strychnine–sensitive glycine receptors. J Biol Chem. 2005; 280:37877–37884. [PubMed: 16144831]
24. Harvey RJ, Thomas P, James CH, Wilderspin A, Smart TG. Identification of an inhibitory Zn^{2+} binding site on the human glycine receptor alpha1 subunit. J Physiol. 1999; 520:53–64. [PubMed: 10517800]
25. Nevin ST, et al. Insights into the structural basis for zinc inhibition of the glycine receptor. J Biol Chem. 2003; 278:28985–28992. [PubMed: 12740384]
26. Miller PS, Beato M, Harvey RJ, Smart TG. Molecular determinants of Glycine receptor {alpha}{beta}subunit sensitivities to Zn2+ inhibition. J Physiol. 2005

27. Celie PH, et al. Crystal structure of nicotinic acetylcholine receptor homolog AChBP in complex with an alpha–conotoxin PnIA variant. Nat Struct Mol Biol. 2005; 12:582–588. [PubMed: 15951818]
28. Fu DX, Sine SM. Asymmetric contribution of the conserved disulfide loop to subunit oligomerization and assembly of the nicotinic acetylcholine receptor. J Biol Chem. 1996; 271:31479–31484. [PubMed: 8940161]
29. Sali A, Blundell TL. Comparative protein modelling by satisfaction of spatial restraints. J Mol Biol. 1993; 234:779–815. [PubMed: 8254673]
30. Han NL, Haddrill JL, Lynch JW. Characterization of a glycine receptor domain that controls the binding and gating mechanisms of the beta–amino acid agonist, taurine. J Neurochem. 2001; 79:636–647. [PubMed: 11701767]
31. Laube B, Kuhse J, Betz H. Kinetic and mutational analysis of Zn2+ modulation of recombinant human inhibitory glycine receptors. J Physiol. 2000; 522(Pt 2):215–230. [PubMed: 10639099]
32. Auld DS. Zinc coordination sphere in biochemical zinc sites. Biometals. 2001; 14:271–313. [PubMed: 11831461]
33. Cashin AL, Torrice MM, McMenimen KA, Lester HA, Dougherty DA. Chemical–scale studies on the role of a conserved aspartate in preorganizing the agonist binding site of the nicotinic acetylcholine receptor. Biochemistry. 2007; 46:630–639. [PubMed: 17223685]
34. Lerma J, Zukin RS, Bennett MV. Glycine decreases desensitization of N–methyl–D–aspartate (NMDA) receptors expressed in Xenopus oocytes and is required for NMDA responses. Proc Natl Acad Sci U S A. 1990; 87:2354–2358. [PubMed: 1690430]
35. Grudzinska J, et al. The beta subunit determines the ligand binding properties of synaptic glycine receptors. Neuron. 2005; 45:727–739. [PubMed: 15748848]
36. Wilkins ME, Smart TG. Redox modulation of GABAA receptors obscured by Zn2+ complexation. Neuropharmacology. 2002; 43:938–944. [PubMed: 12423663]
37. Beato M, Groot–Kormelink PJ, Colquhoun D, Sivilotti LG. Openings of the rat recombinant alpha 1 homomeric glycine receptor as a function of the number of agonist molecules bound. J Gen Physiol. 2002; 119:443–466. [PubMed: 11981023]
38. Shen MY, Sali A. Statistical potential for assessment and prediction of protein structures. Protein Sci. 2006; 15:2507–2524. [PubMed: 17075131]
39. Creighton TE. The energetic ups and downs of protein folding. Nat Struct Biol. 1994; 1:135–138. [PubMed: 7656027]
40. Yaron A, Naider F. Proline–dependent structural and biological properties of peptides and proteins. Crit Rev Biochem Mol Biol. 1993; 28:31–81. [PubMed: 8444042]
41. Mukhtasimova N, Sine SM. An intersubunit trigger of channel gating in the muscle nicotinic receptor. J Neurosci. 2007; 27:4110–4119. [PubMed: 17428989]
42. Kash TL, Jenkins A, Kelley JC, Trudell JR, Harrison NL. Coupling of agonist binding to channel gating in the GABA(A) receptor. Nature. 2003; 421:272–275. [PubMed: 12529644]
43. Lee WY, Sine SM. Principal pathway coupling agonist binding to channel gating in nicotinic receptors. Nature. 2005; 438:243–247. [PubMed: 16281039]
44. Lummis SC, et al. Cis–trans isomerization at a proline opens the pore of a neurotransmitter–gated ion channel. Nature. 2005; 438:248–252. [PubMed: 16281040]
45. Boileau AJ, Newell JG, Czajkowski C. GABA(A) receptor beta 2 Tyr97 and Leu99 line the GABA–binding site. Insights into mechanisms of agonist and antagonist actions. J Biol Chem. 2002; 277:2931–2937. [PubMed: 11711541]
46. Chakrapani S, Bailey TD, Auerbach A. The role of loop 5 in acetylcholine receptor channel gating. J Gen Physiol. 2003; 122:521–539. [PubMed: 14557402]
47. Grosman C, Zhou M, Auerbach A. Mapping the conformational wave of acetylcholine receptor channel gating. Nature. 2000; 403:773–776. [PubMed: 10693806]
48. Padgett CL, Hanek AP, Lester HA, Dougherty DA, Lummis SC. Unnatural amino acid mutagenesis of the GABA(A) receptor binding site residues reveals a novel cation–pi interaction between GABA and beta 2Tyr97. J Neurosci. 2007; 27:886–892. [PubMed: 17251430]

49. Henchman RH, Wang HL, Sine SM, Taylor P, McCammon JA. Ligand–induced conformational change in the alpha7 nicotinic receptor ligand binding domain. Biophys J. 2005; 88:2564–2576. [PubMed: 15665135]
50. Schmieden V, Kuhse J, Betz H. A novel domain of the inhibitory glycine receptor determining antagonist efficacies: further evidence for partial agonism resulting from self–inhibition. Mol Pharmacol. 1999; 56:464–472. [PubMed: 10462533]
51. Chang Y, Weiss DS. Site–specific fluorescence reveals distinct structural changes with GABA receptor activation and antagonism. Nat Neurosci. 2002; 5:1163–1168. [PubMed: 12368804]
52. Paoletti P, Ascher P, Neyton J. High–affinity zinc inhibition of NMDA NR1–NR2A receptors. J Neurosci. 1997; 17:5711–5725. [PubMed: 9221770]
53. Colquhoun D, Sakmann B. Fast events in single–channel currents activated by acetylcholine and its analogues at the frog muscle end–plate. J Physiol. 1985; 369:501–557. [PubMed: 2419552]
54. Thompson JD, Higgins DG, Gibson TJ. CLUSTAL W: improving the sensitivity of progressive multiple sequence alignment through sequence weighting, position–specific gap penalties and weight matrix choice. Nucleic Acids Res. 1994; 22:4673–4680. [PubMed: 7984417]
55. Shindyalov IN, Bourne PE. Protein structure alignment by incremental combinatorial extension (CE) of the optimal path. Protein Eng. 1998; 11:739–747. [PubMed: 9796821]
56. Pettersen EF, et al. UCSF Chimera—a visualization system for exploratory research and analysis. J Comput Chem. 2004; 25:1605–1612. [PubMed: 15264254]
57. Canutescu AA, Shelenkov AA, Dunbrack RL Jr. A graph–theory algorithm for rapid protein side–chain prediction. Protein Sci. 2003; 12:2001–2014. [PubMed: 12930999]
58. Davis IW, et al. MolProbity: all–atom contacts and structure validation for proteins and nucleic acids. Nucleic Acids Res. 2007; 35:W375–W383. [PubMed: 17452350]
59. Jones DT. Protein secondary structure prediction based on position–specific scoring matrices. J Mol Biol. 1999; 292:195–202. [PubMed: 10493868]
60. Miesenbock G, De Angelis DA, Rothman JE. Visualizing secretion and synaptic transmission with pH–sensitive green fluorescent proteins. Nature. 1998; 394:192–195. [PubMed: 9671304]

Europe PMC Funders Author Manuscripts

Europe PMC Funders Author Manuscripts

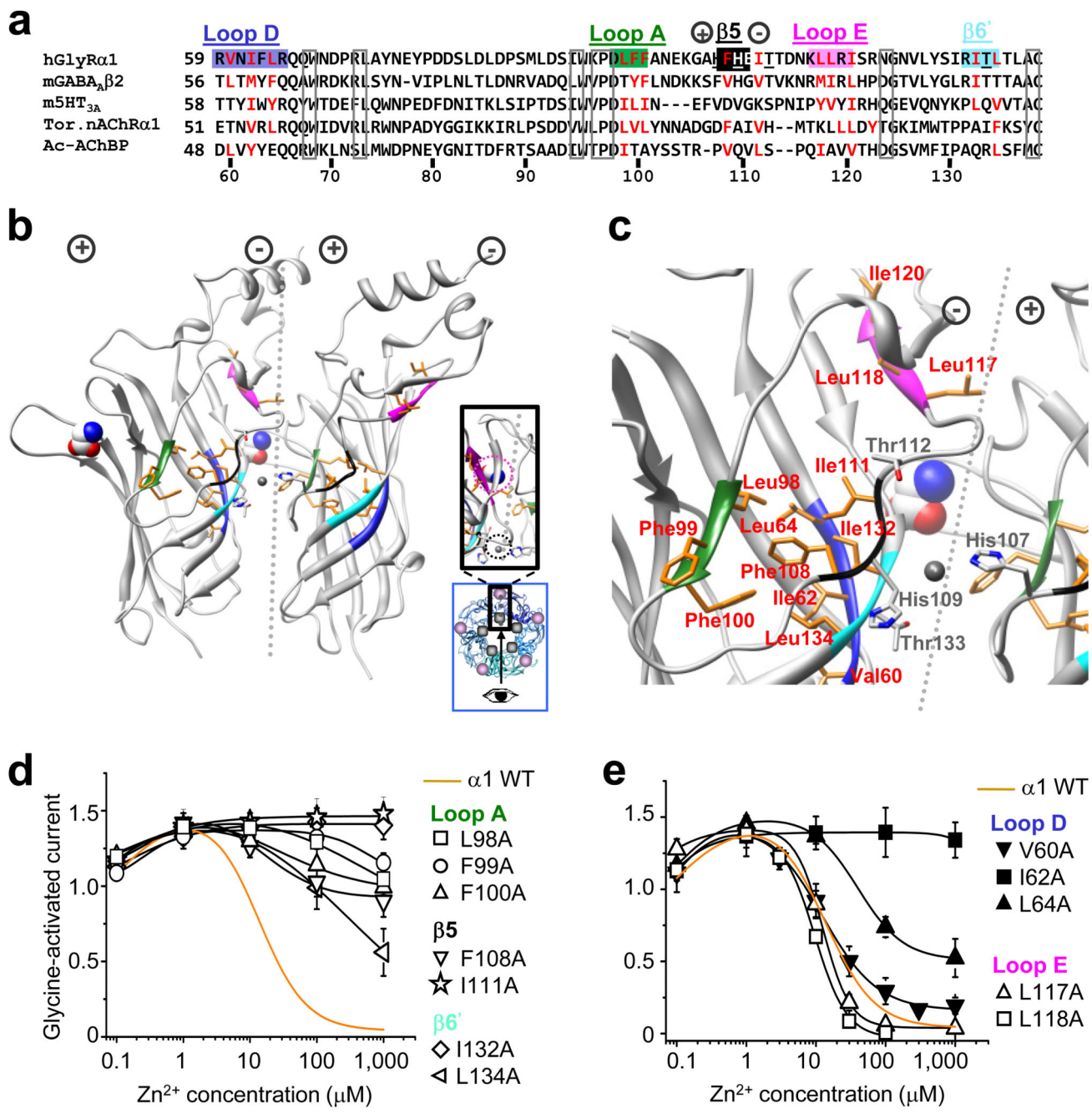

Figure 1. Hydrophobic determinants of Zn^{2+} inhibition.

(**a**) Partial protein alignment of Cys–loop receptor ECDs showing: GlyR α1 hydrophobic residues that are examined (red); where hydrophobicity is retained in other Cys–loop receptors (red); conserved residues (boxed); and the GlyR Zn^{2+} inhibition binding site residues (underlined). Hydrophobic motifs are labelled and colour–coded in accordance with **(b, c)**, the GlyR α1 ECD homology model based on *Tor*nAChRα$_1$ [1]. Clustered hydrophobic residues (orange) connect the Zn^{2+} inhibition site at the inner–subunit interface (black and light blue motifs – note, black motif is not a β–strand in the model but referred to as such in

Europe PMC Funders Author Manuscripts

main text for clarity [2]), to glycine binding loops A (green), D (dark blue) and E (mauve) of outer–subunit interface. Zn^{2+} inhibition site residues, His^{107}, His^{109}, Thr^{112} and Thr^{133}, are in grey (nitrogen atoms are blue and oxygens are red). Dotted line depicts the interface with (+) and (–) subunit sides [28]. Glycine, displayed in CPK, spacefill, was fitted manually in accordance with [35]; Zn^{2+}, fitted manually, in grey, spacefill. Exact side chain orientations presented here are speculative, based on best alignment and modelling estimations. Inset, blue box – pentamer plan view showing viewing angle (arrow) for main picture, and revealing the separation between the Zn^{2+} binding site (grey circle) and glycine binding site (mauve circle); enlarged plan view of interface shown in black box. **(d, e)** Zn^{2+} concentration response curves for modulation of EC_{50} glycine currents on wild–type (WT; dashed line) and alanine–substituted receptors. $\alpha1^{I120A}$ did not traffic to cell surface so no recordings were made (Supplementary Figure 2). Curves fitted with Hill equation. All points are means ± s.e.m. (n = 3–6).

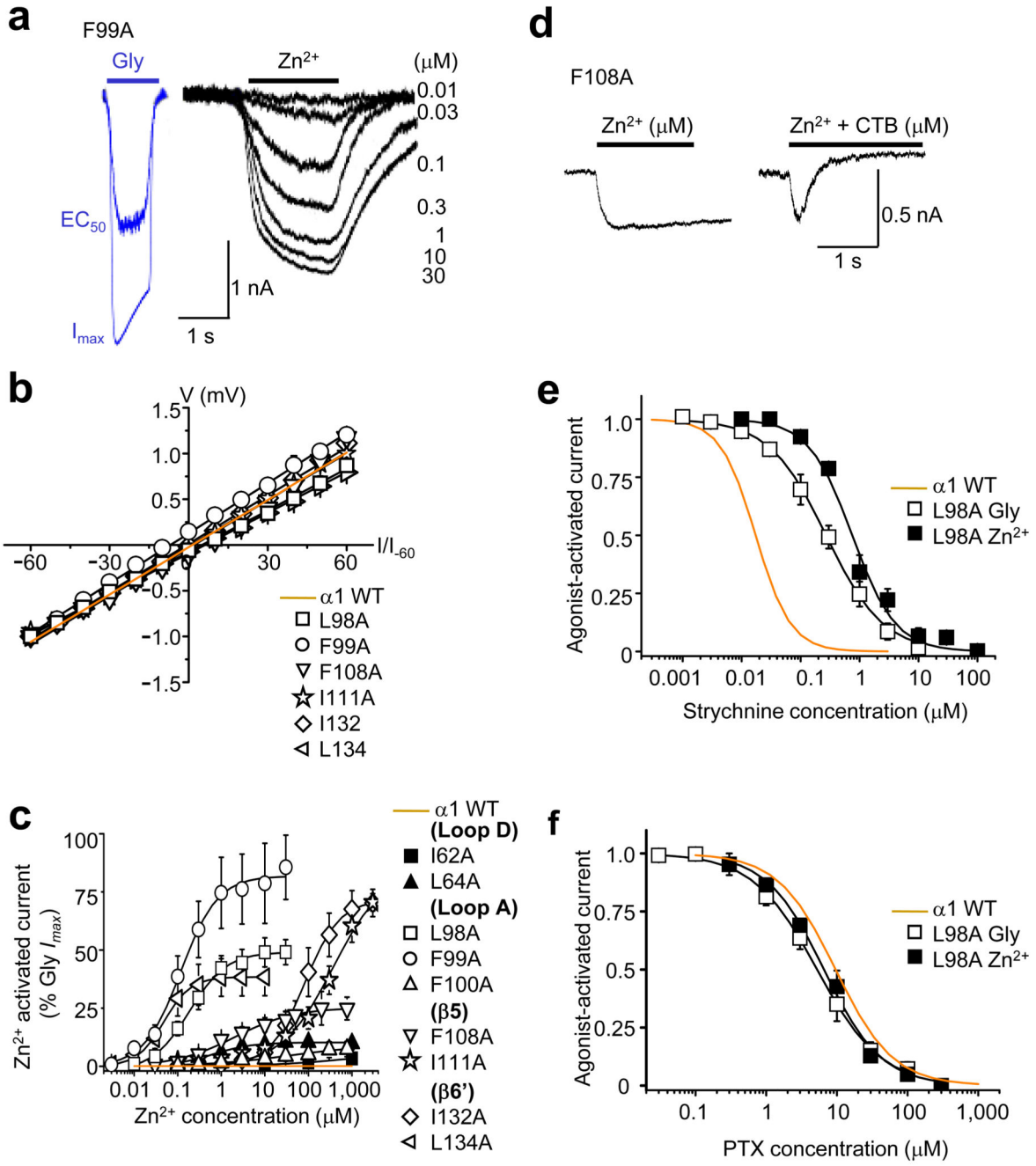

Figure 2. Direct Zn^{2+} activation of substituted GlyRs.

(a) Representative glycine currents (blue traces) in the absence of Zn^{2+} (EC_{50} – 30 μM; I_{max} – 1000 μM) and Zn^{2+} currents (black traces) in absence of glycine (0.01 – 30 μM) for GlyR $\alpha1^{F99A}$. **(b)** Zn^{2+} current–voltage (I–V) relationships (normalised to the current recorded at –60 mV and fitted by linear regression) for the six most efficacious ZAGs, where EC_{50} Zn^{2+} responses were large enough to be recorded reliably, and for the wild–type (WT) receptor. **(c)** Zn^{2+} activation–response curves for alanine–substituted GlyRs; Zn^{2+} maxima are normalised to glycine maxima (10 mM) in same cell. **(d)** Representative $\alpha1^{F108A}$ Zn^{2+} I_{max}

(100 μM) current co–applied with and without 20 μM CTB. Inhibition greater than 100% is due to additional background leak (discussed later in Fig. 6). **(e, f)** $\alpha 1^{L98A}$ concentration inhibition curves for strychnine and picrotoxin, respectively on glycine or Zn^{2+} EC_{50}–activated currents (n = 3 –6). Wild–type receptor activation sensitivities to the antagonists are shown in orange.

Europe PMC Funders Author Manuscripts

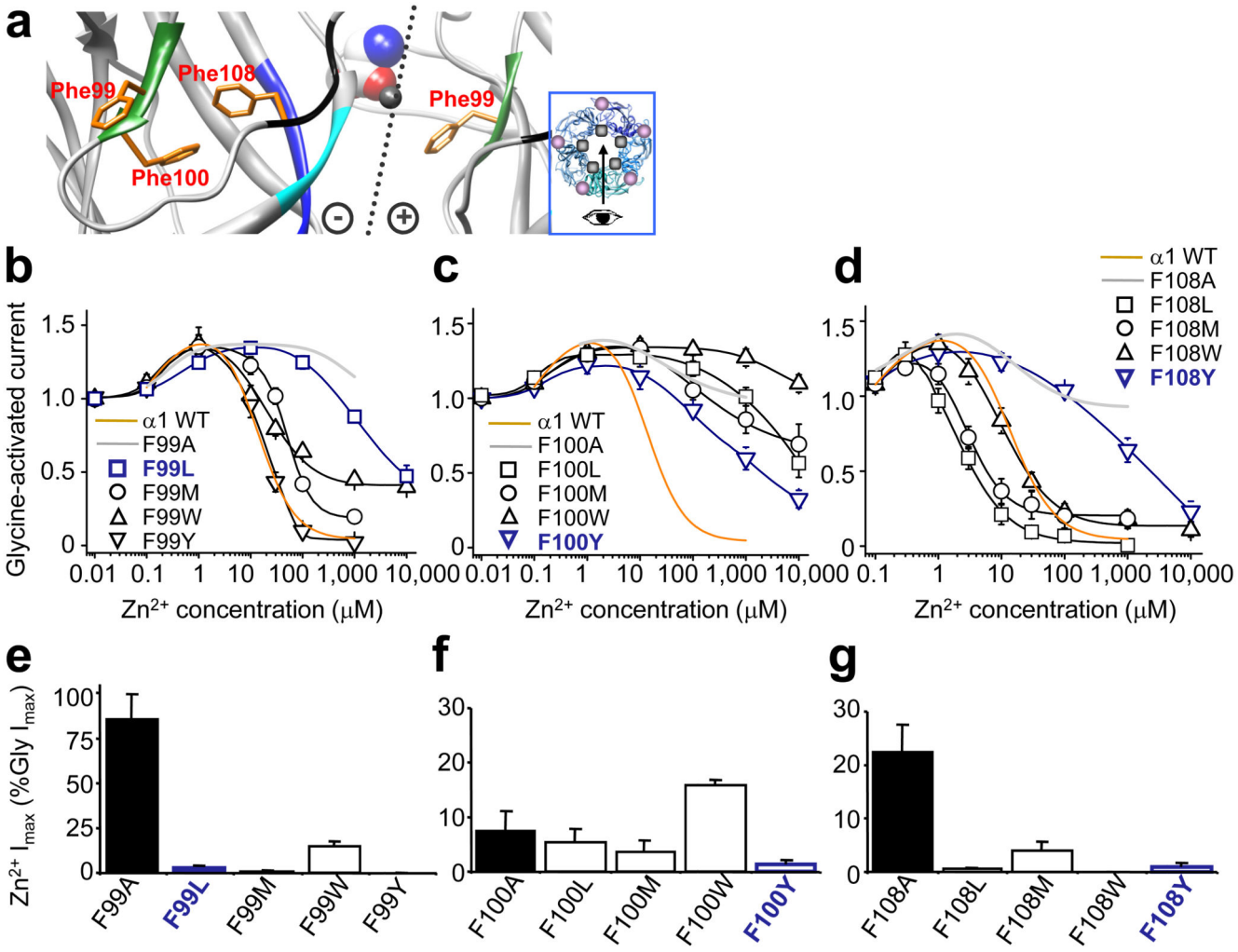

Figure 3. Zn^{2+} inhibition and Zn^{2+} activation in GlyRs with conservative substitutions.

(a) Homology model showing Phe99 and Phe100 from glycine binding loop A (green) and Phe108 from β5 strand of Zn^{2+} inhibition site (black). Dotted line: interface with (+) and (–) subunit sides [28]. Glycine (CPK, spacefill) was docked manually [35]; Zn^{2+} (representation only, grey spacefill). Inset – pentamer plan viewing angle (arrow), Zn^{2+} binding site (grey spot), glycine binding site (mauve spot). **(b–d)** Zn^{2+} concentration response curves for modulation of EC_{50} glycine currents from GlyRs with conservative hydrophobic substitutions at positions Phe99 **(b)**, Phe100 **(c)**, and Phe108 **(d).** For comparison, wild–type (WT) inhibition profiles (orange) and alanine substituted receptor profiles (grey) are included. The same set of substituted GlyRs were assessed for maximal Zn^{2+} (1 mM)–activated currents (I_{max}), normalised to glycine I_{max} (10 mM) in the same cell: Phe99 **(e)**, Phe100 **(f)** and Phe108 **(g)**. Alanine substituted receptor Zn^{2+} I_{max} (black bars) is shown for comparison. Note: F99L, F100Y and F108Y had substantially attenuated Zn^{2+} inhibition (navy blue lines) but almost no Zn^{2+} activation (navy blue bars; < 2% Gly I_{max}). (n = 3 – 6)

Europe PMC Funders Author Manuscripts

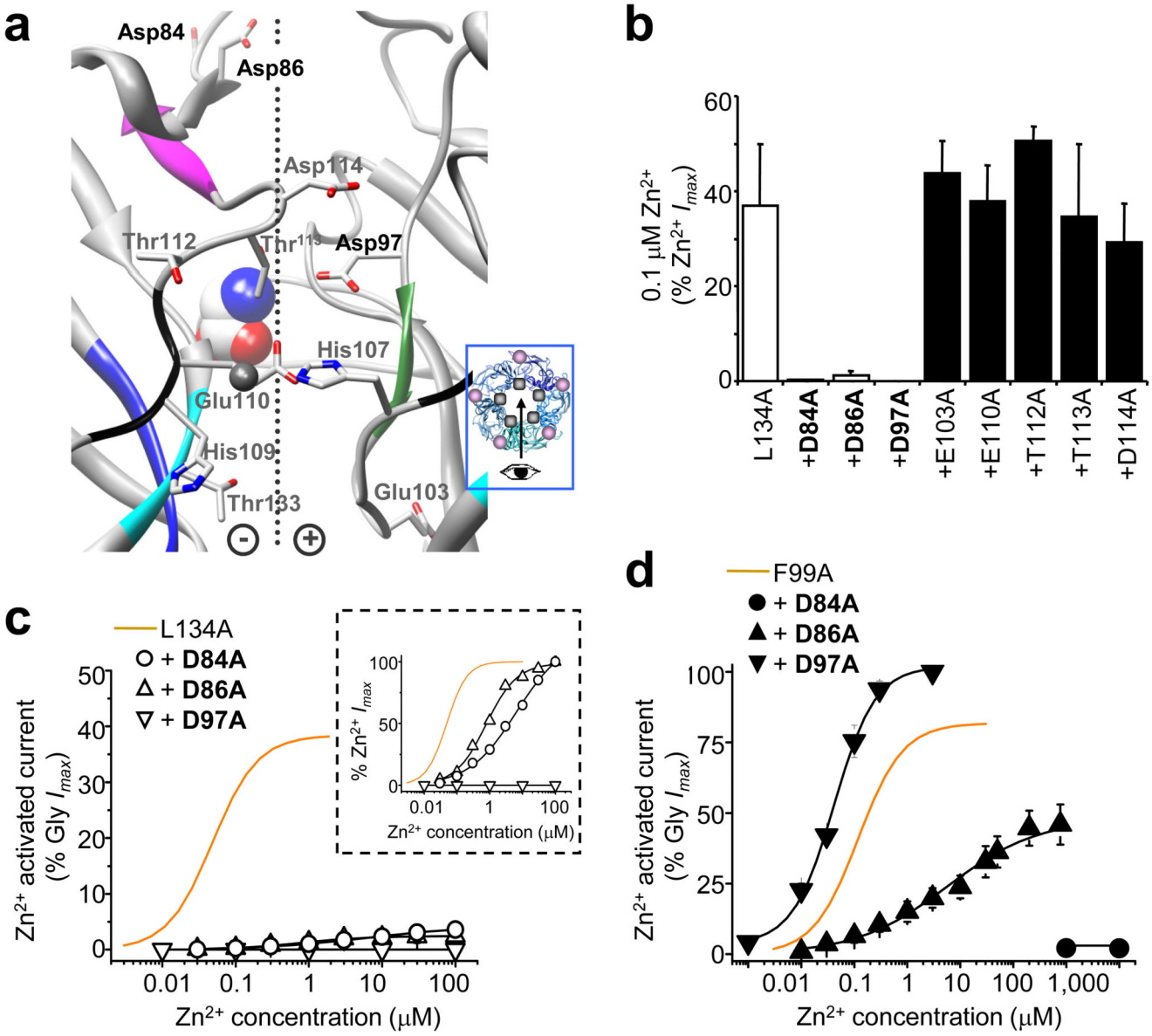

Figure 4. Identifying potential residues for the Zn^{2+} activation binding site in ZAGs.

(a) Homology model showing potential Zn^{2+} coordinating residues at the subunit interface around the His107 /His109 /Thr112 /Thr133 Zn^{2+} inhibition site. Side chains in grey, nitrogens in blue, oxygens in red. Dotted line: interface with (+) and (–) sides [28]. Glycine (CPK, spacefill) was docked manually [35]; Zn^{2+} (representation only, grey, spacefill). Inset shows the viewing angle (arrow), with Zn^{2+} (grey spot) and glycine binding sites (mauve spot). **(b)** 0.1μM Zn^{2+}–activation of alanine–substituted $\alpha1^{L134A}$ background GlyRs, expressed as a percentage Zn^{2+} I_{max} in the same cell. **(c)** Zn^{2+} activation concentration response curves for $\alpha1^{L134A, D84A}$, $\alpha1^{L134A, D86A}$ and $\alpha1^{L134A, D97A}$ receptors normalised to the Gly I_{max} and also normalised to the Zn^{2+} I_{max} (inset). **(d)** Zn^{2+} activation response curves for the equivalent mutations on an $\alpha1^{F99A}$ background showing that although Asp84 and Asp86 are still required for Zn^{2+} activation, Asp97 is not. (n = 3–6).

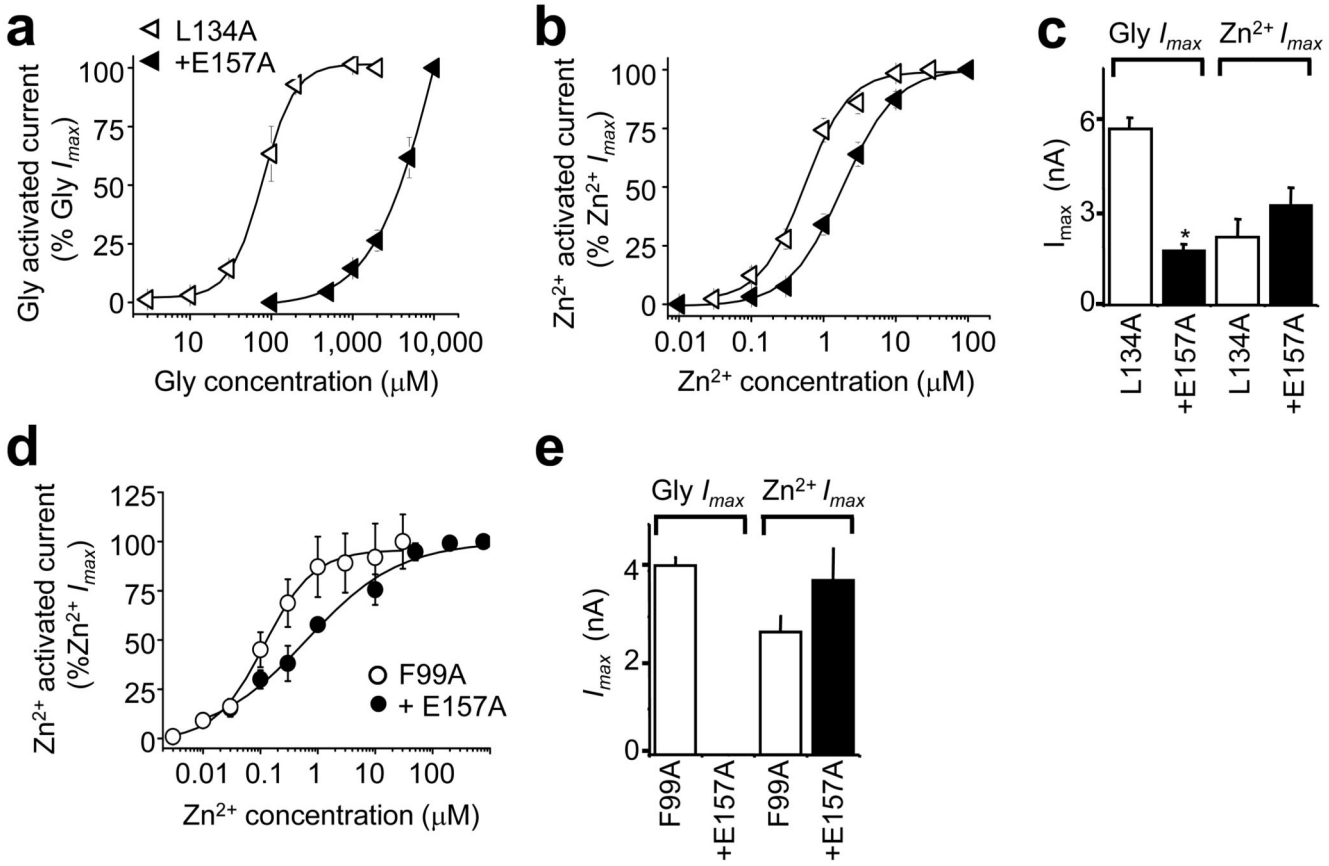

Figure 5. Zn^{2+}–activation of GlyRs lacking a high affinity glycine binding site.

Glycine (a) and Zn^{2+} (b) concentration response curves on an $\alpha1^{L134A}$ background with an extra mutation in the glycine binding site (E157A). (c) Maximum currents evoked by glycine (10 mM) and Zn^{2+} (1 mM) for $\alpha1^{L134A}$ and $\alpha1^{L134A, E157A}$. Incorporating E157A on an $\alpha1^{F99A}$ background, ablated activation by up to 10 mM glycine, but induced only a modest, 3–fold decrease in sensitivity to Zn^{2+} activation (d) and no reduction in Zn^{2+} I_{max} (1 mM) (e) (n = 3–4).

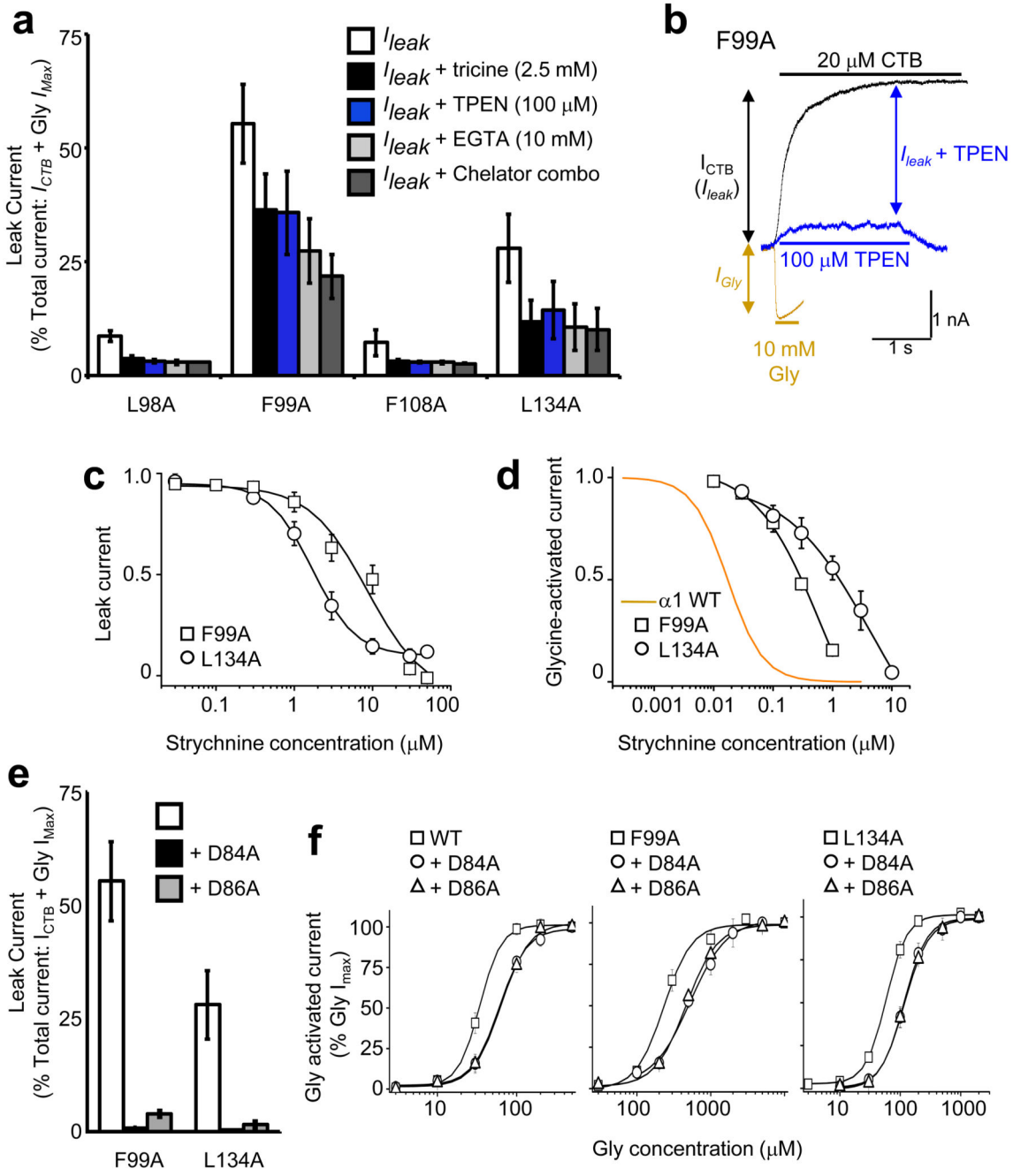

Figure 6. Spontaneous activation of alanine–substituted receptors.

(a) Persistent leak currents for alanine substituted GlyRs (= % CTB blockable current (I_{CTB})/(I_{CTB} + Gly I_{Max})) in presence of individual and combined ion chelators. **(b)** Membrane currents for $\alpha1^{F99A}$ ZAG in the presence of either glycine (orange), CTB (black) or TPEN (blue), overlaid to demonstrate their relative contributions to the total current **(c)** Strychnine concentration curves for inhibiting leak currents for $\alpha1^{F99A}$ and $\alpha1^{L134A}$ ZAGs **(c)** and EC_{50} glycine–activated current **(d)**. Orange line indicates strychnine concentration inhibition curve for WT GlyRs, which are notably more sensitive as the agonist binding

loops A and D are not perturbed. **(e)** Persistent leak current absent from receptors with alanine substitutions at Asp84 or Asp86 on $\alpha1^{F99A}$ and $\alpha1^{L134A}$ backgrounds. **(f)** Glycine sensitivity is modestly reduced in alanine–substituted Asp84 or Asp86 receptors, as compared to wild–type, $\alpha1^{F99A}$ and $\alpha1^{L134A}$ backgrounds. n = 3 –6.

Europe PMC Funders Author Manuscripts

Europe PMC Funders Author Manuscripts

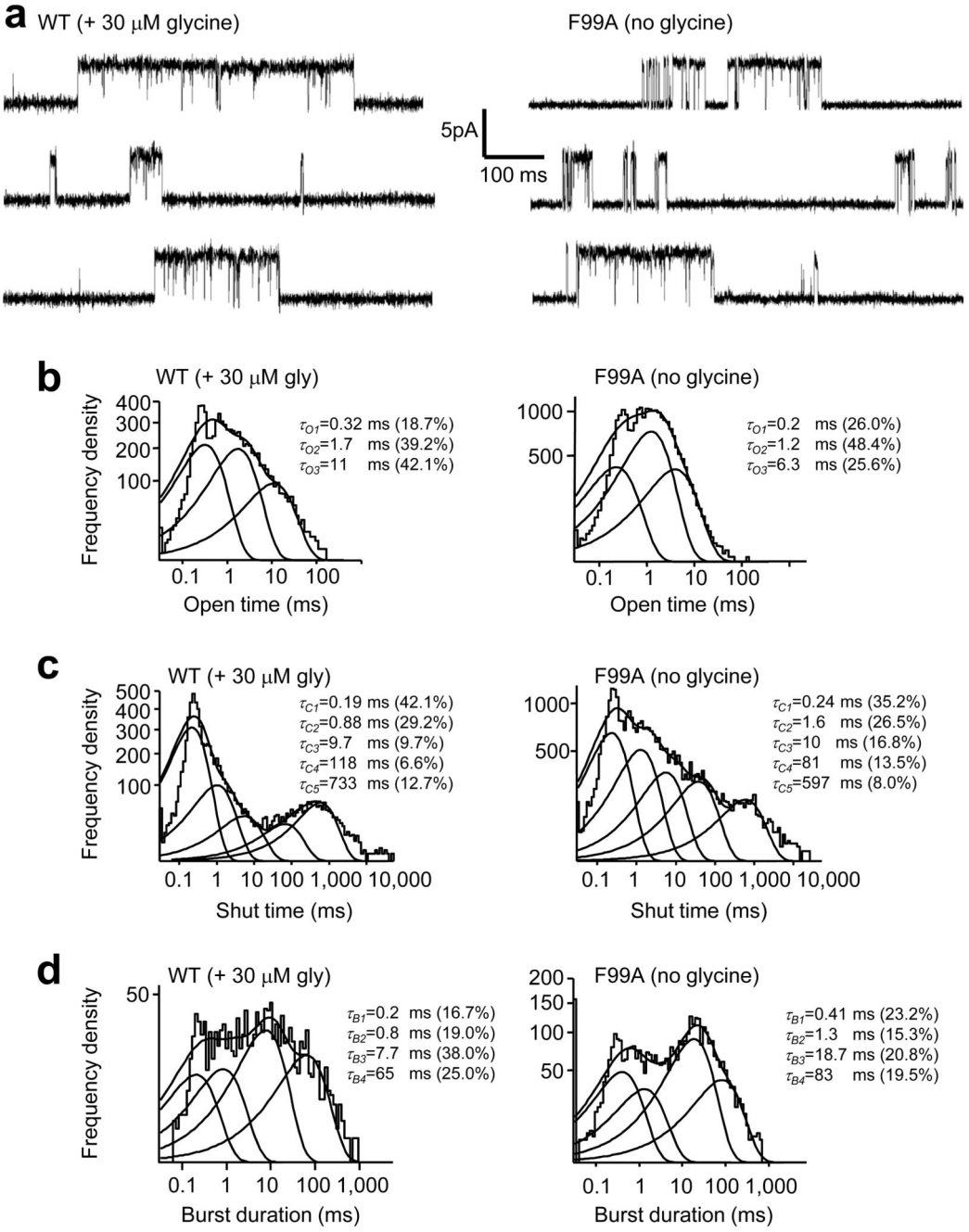

Figure 7. Spontaneous channel activation mimics agonist–induced activation.

(a) Single channel currents from cell–attached recordings of HEK cells expressing either WT α1 GlyRs or GlyR α1F99A, at a pipette potential +60 mV. Burst activity was recorded in the presence of glycine (EC_{30}) for WT and in its absence for spontaneously–activated $\alpha1^{F99A}$. TPEN (100 μM) was present in the pipette solution to remove contaminating Zn^{2+}. **(b–d)** Dwell time distributions for **(b)** open times, **(c)** shut times, and **(d)** burst durations.

Europe PMC Funders Author Manuscripts

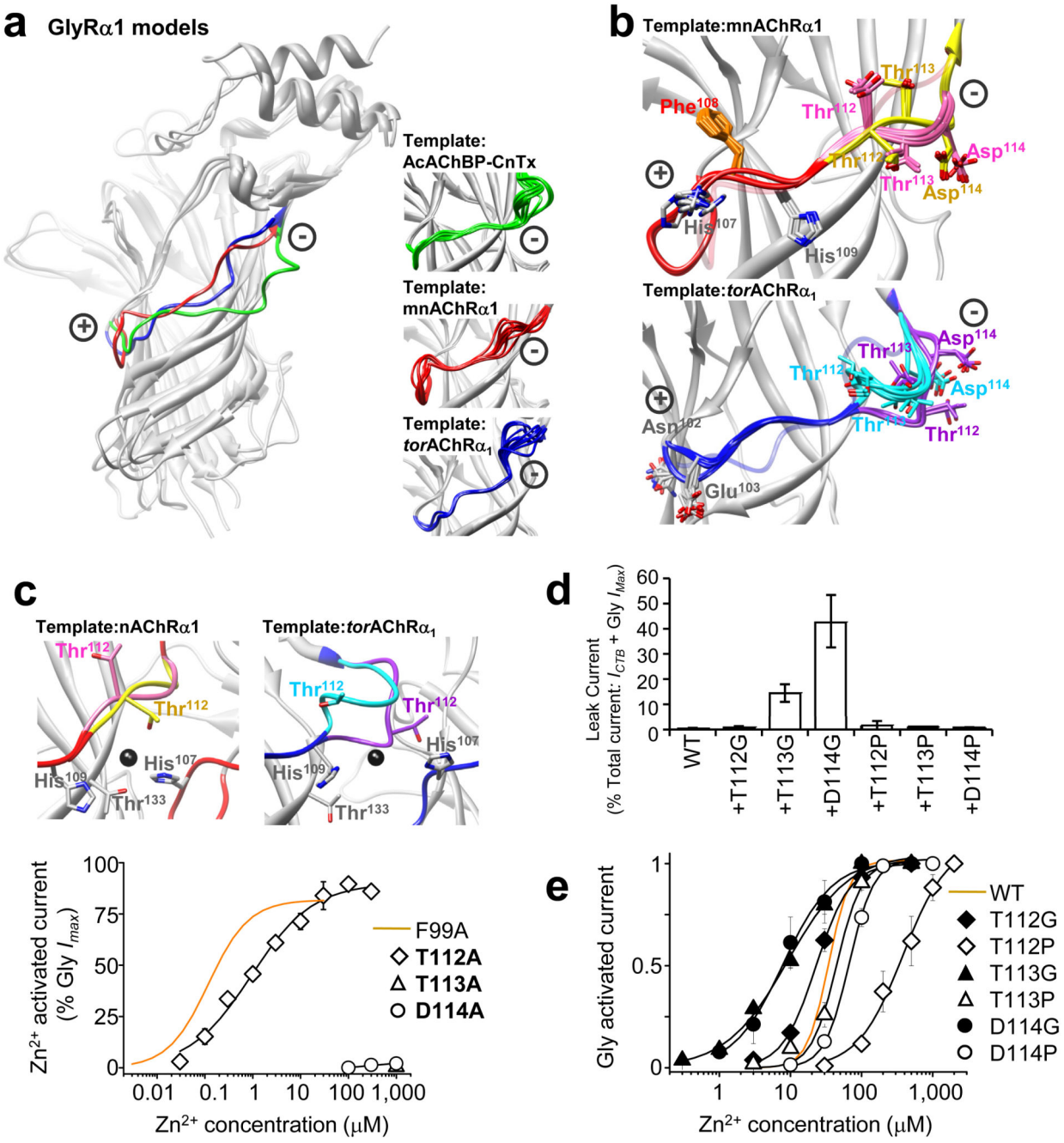

Figure 8. Zn^{2+} and spontaneous channel activation originates *via* the Zn^{2+} inhibition site '–' loop face.

(a) CE structural alignments [55] of GlyR α1 homology models based on three predicted 'closed' conformation templates. Note, structural variability at the Zn^{2+} inhibition site (+) and (–) faces between the conotoxin–bound Ac–AChBP [27] (green), mnAChR α1 [14] (red) and *Tom*AChR α_1 [1] (blue) templates. **(a – insets)** Overlays of 10 lowest energy models for each template reveal particular uncertainty over the fitting of the (–) face but less uncertainty for the (+) face. (**b)** 10 lowest energy loop conformations resulting from DOPE loop

refinement [38] of the (+) and (–) Zn^{2+} inhibition site loops starting from the best GlyR α1 model based on two different templates. This revealed one favourable conformation for the (+) face loop for each template–derived model, with only minor deviations in the peptide backbone (red) and side chain positions between models. In contrast, multiple peptide backbone conformations were equally preferred for the (–) face loop (pink or yellow for mnAChR α1; aquamarine or purple for *Tom*AChR α_1) with clear divergence in side chain positions. Original model backbone conformations before loop refinement are shown in translucent red (mnAChR α1) and translucent blue (*Tom*AChR α_1). **(c)** Zn^{2+} activation–response curves from GlyRs with potential Zn^{2+} coordinating residues on the (+) and (–) inhibition site faces substituted with alanines; Zn^{2+} maxima normalised to glycine maximal current (10 mM) in same cell. Only $\alpha1^{T112A}$ exhibited highly–sensitive and efficacious ZAG activity. ZAG $\alpha1^{F99A}$ (orange line; originally from Fig. 2c) included for comparison. **Insets:** DOPE loop refinement of GlyR α1 models from mnAChR α1 and *Tom*AChR α_1 templates show how alternate favourable conformations on the (–) face loop could have a substantive impact on the organisation of Thr112 in the Zn^{2+} binding site. Zn^{2+} (fitted manually, dark grey, spacefill). **(d)** Significant spontaneous activity, measured as persistent leak currents ($I_{CTB}/(I_{CTB}$ + Gly I_{Max})) in the presence of 100 μM TPEN, was observed for GlyR $\alpha1^{T113G}$ and $\alpha1^{D114G}$ where '–' loop flexibility was increased, but not for GlyR $\alpha1^{T113P}$ and $\alpha1^{D114P}$ where flexibility was reduced. **(e)** Glycine concentration response curves for receptors with glycine or proline substitutions at positions 112, 113 or 114 in the '–' loop. Glycine increased agonist sensitivity compared to proline substitution at the equivalent position. Glycine curve for WT receptors included for comparison (orange line; n = 3–7).

Europe PMC Funders Author Manuscripts

Table 1

Glycine activation, Zn^{2+} modulation and Zn^{2+} activation data from wild-type (WT) receptors and from GlyRs carrying alanine substitutions of hydrophobic residues at positions running from the Zn^{2+}inhibition site to nearby agonist binding loops, expressed in HEK cells.

	Glycine				Zn^{2+}				
					Inhibition	Activation			
	EC_{50} (μM)	n_H	I_{max} (nA)	N	IC_{50} (μM)	EC_{50} (μM)	n_H	Relative efficacy (% Gly I_{max})	N
α1 WT	35 ± 5	2.7 ± 0.2	6.8 ± 0.5	6	15 ± 2	None	—	—	4
Agonist binding loop A									
$α1^{L98A}$	35 ± 6	1.9 ± 0.3	6.4 ± 0.5	6	> 1000	0.26 ± 0.08	1.1 ± 0.2	49 ± 5	4
$α1^{F99A}$	250 ± 40	2.3 ± 0.3	3.9 ± 0.4	4	> 1000	0.13 ± 0.03	1.1 ± 0.1	86 ± 13	5
$α1^{F100A}$	120 ± 20	1.8 ± 0.2	4.5 ± 0.7	5	> 1000	9.2 ± 0.6	0.5 ± 0.1	7 ± 4	4
Zn^{2+} binding site: β5 strand									
$α1^{F108A}$	15 ± 3	2.3 ± 0.1	4.5 ± 0.5	5	> 1000	2.3 ± 0.6	0.7 ± 0.1	25 ± 6	6
$α1^{I111A}$	39 ± 4	1.3 ± 0.2	4.6 ± 0.8	4	> 1000	470 ± 130	0.7 ± 0.2	83 ± 3	3
Zn^{2+} binding site: β6' strand									
$α1^{I132A}$	95 ± 15	2.7 ± 0.4	6.1 ± 0.7	6	> 1000	140 ± 30	1.2 ± 0.1	72 ± 5	5
$α1^{L134A}$	58 ± 3	3.0 ± 0.4	6.0 ± 0.3	7	> 1000	0.06 ± 0.01	1.3 ± 0.1	38 ± 9	5
Agonist binding loop Δ									
$α1^{V60A}$	91 ± 15	3.5 ± 0.8	6.5 ± 1.3	4	10.1 ± 1.26	None	—	—	4
$α1^{I62A}$	240 ± 7	2.5 ± 0.1	7.6 ± 0.7	3	> 1000	> 1000	—	3 ± 1	4
$α1^{L64A}$	10 ± 3	2 ± 0.6	5.6 ± 0.8	4	70 ± 9	1.5 ± 1.3	1.1 ± 0.4	10 ± 3	3
Agonist binding loop E									
$α1^{L117A}$	4200 ± 100	1.67 ± 0.1	4.4 ± 0.7	8	13.3 ± 3.3	None	—	—	3
$α1^{L118A}$	1060 ± 110	3.00 ± 0.2	6.3 ± 0.7	3	10.3 ± 0.36	None	—	—	3

Europe PMC Funders Author Manuscripts

Table 2

Data from cell-attached single-channel recordings made from α1 wild-type (WT) or $\alpha1^{F99A}$ receptors expressed in HEK 293 cells. Includes: average durations of open, closed and burst time constants and areas of exponential components that fitted the distributions; single channel amplitudes; P_O for openings within bursts. n = 3. * denotes significant variations between the two receptor populations (P<0.05).

	α1 WT (+30 μM Gly)		**$\alpha1^{F99A}$ (no glycine)**	
Open times	τ_O (ms)	*Area* (%)	τ_O (ms)	*Area* (%)
1	0.28 ± 0.029	36 ± 11	0.4 ± 0.1	36.9 ± 9.3
2	1.5 ± 0.2	39 ± 3	1.7 ± 0.3	41.9 ± 4.0
3	8.9 ± 2.1	26 ± 10	5.2 ± 0.8	21.2 ± 7.2
Closed times	τ_C (ms)	*Area* (%)	τ_C (ms)	*Area* (%)
1	0.22 ± 0.03	44 ± 16	0.26 ± 0.026	37 ± 2
2	0.90 ± 0.24	35 ± 15	1.6 ± 0.17 *	30 ± 3
3	4.3 ± 1.6	8 ± 1	10.0 ± 2.9	18 ± 1 *
4	109 ± 6.2	10 ± 2	89 ± 39	12 ± 1
5	2200 ± 1000	4 ± 1	1200 ± 400	3 ± 3
Burst durations	τ_B (ms)	*Area* (%)	τ_B (ms)	*Area* (%)
1	0.3 ± 0.06	28 ± 7	0.3 ± 0.06	26 ± 2
2	1.4 ± 0.6	22 ± 4	1.4 ± 0.1	22 ± 8
3	6.9 ± 2.2	35 ± 5	17.6 ± 0.8 *	32 ± 8
4	63.4 ± 14.8	19 ± 7	77.1 ± 10.7	20 ± 1
Amplitude (pA)	4.5 ± 0.7		4.1 ± 0.6	
P_O	0.9 ± 0.03		0.53 ± 0.07	